J Appl Electrochem (2014) 44:945–952
DOI 10.1007/s10800-014-0701-3

RESEARCH ARTICLE

A shielded rotating disk setup with improved current distribution

Feng Qiao · Xiaoxuan Sun · Alan C. West

Received: 17 March 2014 / Accepted: 9 June 2014 / Published online: 16 July 2014

Abstract In contrast to wafer-scale experiments that can employ a sophisticated and well-optimized plating tool, coupon-scale studies of electrodeposition can be hindered by poor current distribution. The impact on primary current distribution and mass transfer of an insulating shield that can readily be used in a rotating disk setup is presented. Numerical simulations were employed to design an insulating shield assuming mass-transfer resistances were negligible. Several designs were fabricated and characterized using copper electrodeposition as the electrochemical reaction. Numerical and experimental results are consistent, and the shield is a convenient and effective way to achieve more uniform current distribution. However, the shield disturbs the uniform mass-transfer rates to the substrate surface that are achieved with a rotating disk. Rates are characterized experimentally, and design tradeoffs are discussed.

Keywords Electrodeposition · Current distribution · Uniformity · Shield · Electroplating

List of symbols

r_s	Outer radius of the shield in unit mm
r_{ho}	Inner radius of the shield in unit mm
r_o	Radius of the working electrode in unit mm
i	Local current density in unit mA/cm^2
κ	Electrolyte conductivity in unit S/m
ϕ	Electrical field in the electrolyte
$\boldsymbol{N}$	Normal unit vector
i_c	Applied current density in unit mA/cm^2
A_c	Surface area of the working electrode in unit cm^2
A_a	Surface area of the counter electrode in unit cm^2
Z	Axial coordinate
i_o	Exchange current density in unit mA/cm^2
α_c	Cathodic charge transfer coefficient
F	Faraday constant, 96,485 C/mol
V	Potential on the working electrode in unit V
T	Temperature in unit K
R	Gas constant, 8.314 J/(K mol)
Wa	Wagner number
H	Distance between the anode and the cathode in unit mm
λ_{avg}	Linear average of thickness profile of copper deposit in unit nm
N	Number of data points of each thickness profile
λ_i	Thickness of the copper deposit at ith data point in unit nm
S	Standard deviation of normalized thickness
i_{avg}	Linear average of current–density profile
R	Radial position away from the center in unit mm
K	Slope of Levich plot
N	Number of electrons exchanged in reduction reaction in measuring Levich plots
D	Diffusion coefficient in unit cm^2/s
ω	Rotation speed of RDE in unit rpm
v	Kinematic viscosity in unit cm^2/s
c_∞	Bulk concentration of the Fe(III) complex, 1 mM
i_L	Limiting current density in unit mA/cm^2
t	Thickness of the shield in unit mm

F. Qiao (✉) · X. Sun · A. C. West
Department of Chemical Engineering, Columbia University, New York, NY 10027, USA
e-mail: fq2117@columbia.edu

1 Introduction

Copper, with its low electrical resistivity (1.67 μΩ cm) and good resistance to electromigration, is an important wiring

material for the production of on-chip interconnects. However, in order to follow Moore's law, the required feature size continues to shrink, even below 10 nm [1]. Further reduction of feature sizes will continue to impose stricter requirements on film properties [2]. Additives and operating conditions can have an enormous impact on both mechanical and electrical film properties [3–5], and the need remains for beaker-scale systems to characterize electrodeposition processes as the electrolyte composition is modified [6]. Often, however, such studies are hampered by poor uniformities in film thickness across the substrate [7]. The uniformity of electrodeposited copper film is directly related to the local current density through Faraday's law. While copper films were characterized, the cell can be used to study other electrochemical processes. For example, Lee et al. [6] investigated shielding for MEMS application and showed that the current distribution can be efficiently modified to be more uniform with the use of an insulating shield.

In this study, we improved the design to achieve more uniform current distribution, and we demonstrated that the shielding design can be readily achieved with a rotating disk setup. Copper electrodeposition experiments were carried out on coupon-scale substrates (wafer fragments) to compare with simulation results. Experiments and simulations are in good agreement, in part because we operate at a small fraction of the limiting current density. While plating processes may often be designed to minimize concentration variations of reactant within the electrolyte, the impact of additives may be more significantly influenced by mass-transfer rates [8, 9], which are perturbed by the shield. We thus characterized the overall mass-transfer rate by using a ferri-ferrocyanide redox couple [10], and the spatial variation in mass-transfer rate by copper electropolishing under conditions of mass-transfer control [11].

2 Mathematical Model

Figure 1 shows the schematic diagram of the plating cell with an insulating shield used in the simulation (a) and the actual plating cell setup used for experiments (b). All the geometric parameters shown in Fig. 1 are listed in Table 1. The radius of the exposed area on the wafer coupon r_o was chosen as the characteristic length of the system and was fixed to 10 mm. In the simulations, the other geometric parameters were made dimensionless by dividing by r_o.

Several assumptions are applied to simplify the simulation, while also being consistent with experiment. Most importantly, the electrolyte is assumed to be well mixed. Under such conditions, the current density is given by Ohm's law:

$$i = -\kappa \nabla \phi \tag{1}$$

in which i is the current density, κ is the electrolyte conductivity, and ϕ is the electrical field in the electrolyte. By conservation of charge, the electrical field in the electrolyte is determined by Laplace's equation:

$$\nabla^2 \phi = 0 \tag{2}$$

On any insulating surface such as the wafer holder and the insulating shield, the gradient component of the electrical potential normal to the surface is zero:

$$\boldsymbol{n} \cdot \nabla \phi = 0 \tag{3}$$

in which $\boldsymbol{n}$ is the normal unit vector to the corresponding surface. On the counter electrode (anode) surface, a uniform current density is assumed:

$$\boldsymbol{n} \cdot \nabla \phi = -\frac{i_c \cdot A_c}{\kappa \cdot A_a}, \tag{4}$$

in which i_c is the applied cathodic current density, A_c is the surface area of the working electrode (cathode), and A_a is the surface area of the counter electrode (anode). While it may not be achieved in the experiment, the boundary condition (4) ensures that the desired spatial-average current density is achieved on both the working and counter electrodes. Since the counter electrode is far away from the working electrode, this imposed constraint does not impact the simulated current distribution on the working electrode.

On the working electrode (cathode) surface, Tafel kinetics is assumed:

$$\frac{\partial \phi}{\partial z} = \frac{i_o}{\kappa} \exp\left[-\frac{\alpha_c F(V-\phi)}{RT}\right], \tag{5}$$

in which z is the axial coordinate and its direction is set normal to the working electrode surface, i_o is the exchange current density, α_c is the cathodic charge transfer coefficient, F is Faraday constant, V is the potential on the working electrode, T is the temperature, and R is the gas constant. We assume that the substrate is an ideal conductor (i.e., no terminal effect [12] so that V is constant)

Simulation results depend only on the geometric parameters as well as the Tafel Wagner number of the system, which as described by Newman [13], can be given by

$$Wa_T = \frac{\kappa RT}{|i_c|\alpha_c r_o F} \tag{6}$$

in which the working electrode radius r_o is taken as the characteristic length of the system.

A boundary element method (BEM) validated, for example, by Lee et al. [6] was employed for the simulation. As shown in Fig. 1a, the simulation was carried out by

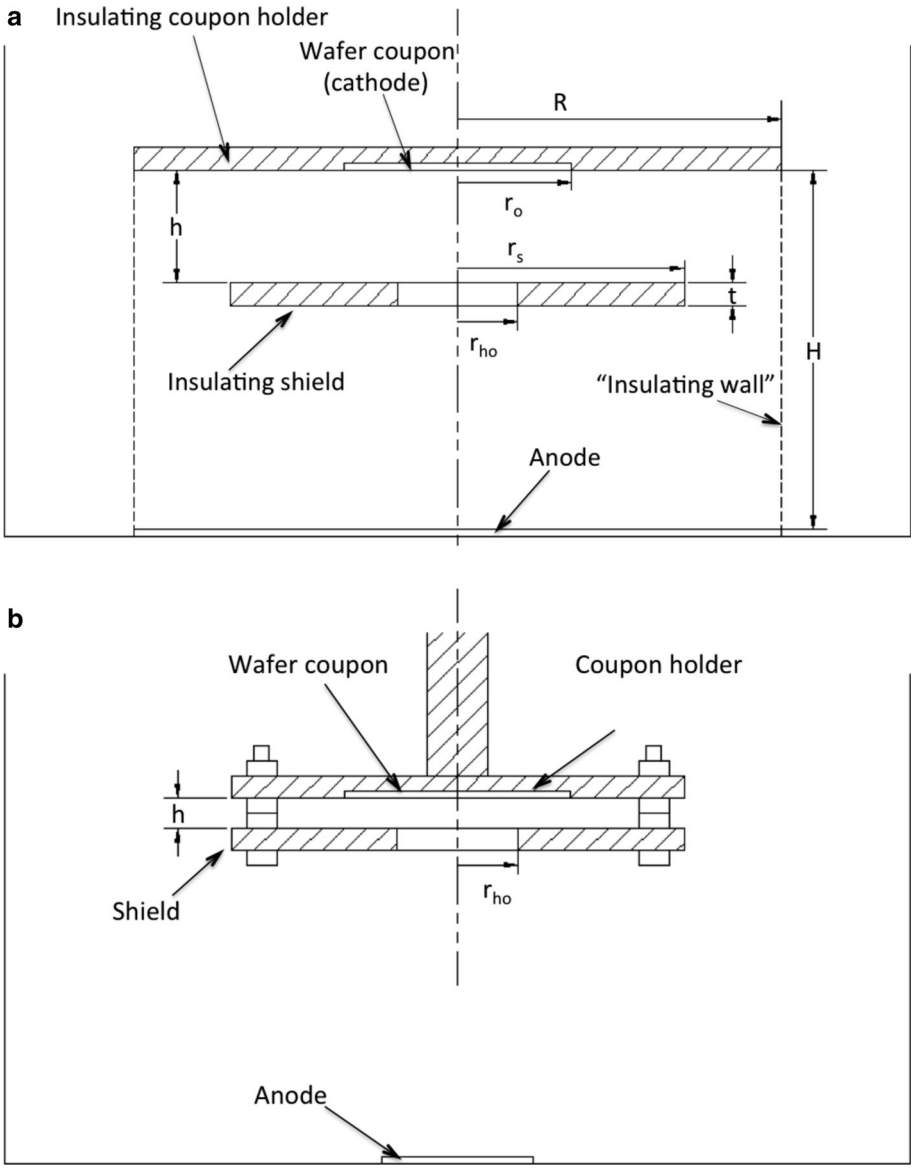

Fig. 1 The schematic diagram of the plating cell with an insulating shield used in simulation (**a**) and the actual plating cell setup used for experiments (**b**)

assuming an axisymmetric problem in a cylindrical computational region with a dimensionless radius of 5 and an overall height corresponding also to a dimensionless distance of 5. The computational region thus consists of eight sub-regions: the anode surface, the cathode surface, the insulating coupon holder surface, the surface of a hypothetical "insulating wall", and the four surfaces (upper, lower, outer, and inner) of the insulating shield. On the cathode surface, 100 node points were used (and constant elements were assumed [6]). On the insulator region next to the cathode, 100 node points were used for $1 < r/r_o < 2$, and an additional 100 node points were used for $2 < r/r_o < 5$. Along all other surfaces, only 20 nodes were used on each of them, and numerical experiments confirmed that this sparse spacing had insignificant impact on calculated current distribution. Once the sets of equations were generated in matrix form, Gaussian elimination using the subroutine MATINV [13] was used for solving the system of equations.

Table 1 Geometric parameters for the plating cell with an insulating shield

Geometric parameter	Value (mm)
Radius of the insulating coupon holder, R	50
Distance between the anode and the cathode, H	50
Radius of the shield, r_s	30
Thickness of the shield, t	3
Radius of exposed area on the wafer coupon, r_o	10
Radius of inner circular hole of the shield, r_{ho}	To be optimized
Distance between the shield and the wafer coupon surface, h	To be optimized

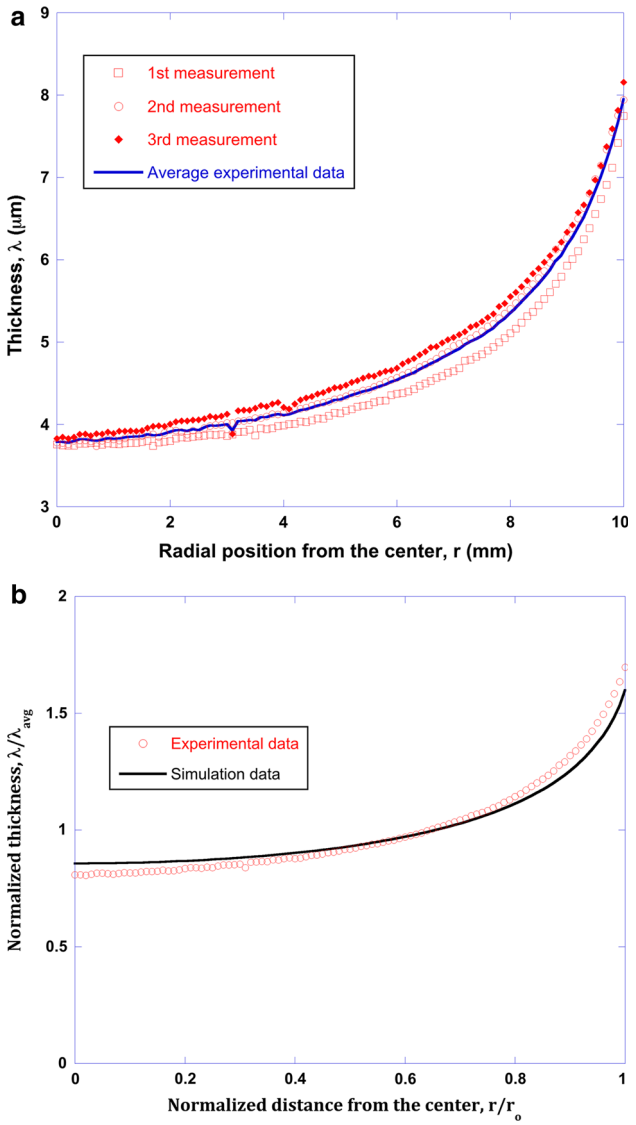

Fig. 2 **a** Three measurements of the deposit thickness profile on a single sample. "Average experimental data" represent the average of the above three measurements. The sample was deposited without a shield at $Wa = 0.394$. **b** Comparison between normalized experimental data and normalized simulation data for current distribution. $Wa = 0.394$

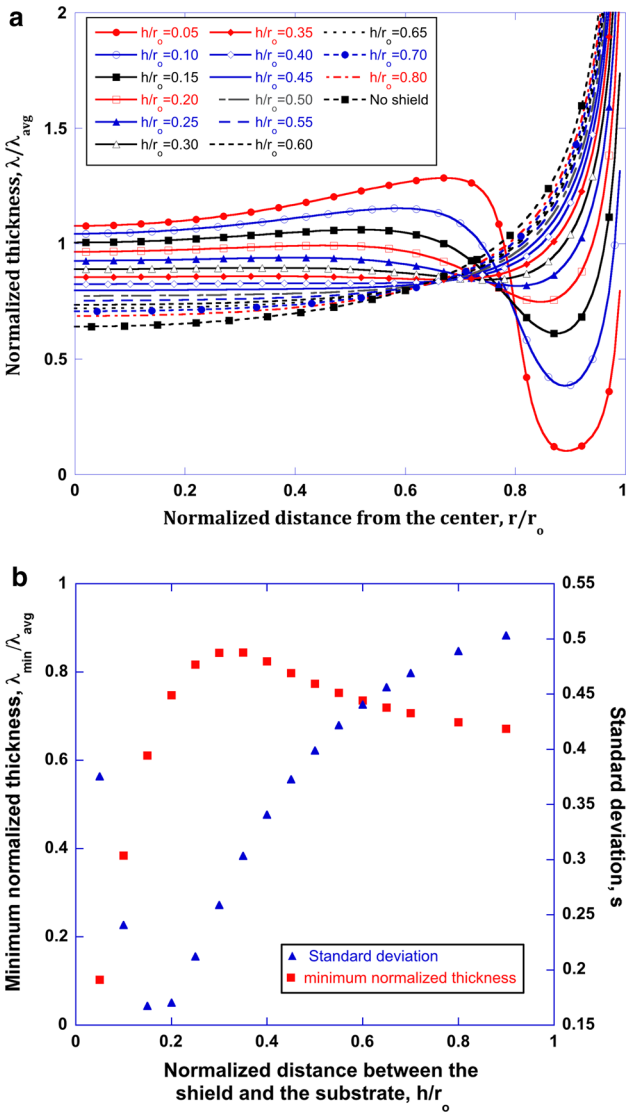

Fig. 3 **a** Normalized thickness profiles for different shield-to-substrate distances assuming $Wa = 0$. For reference, results are also shown for a primary current distribution on a disk without a shield. The radius of the inner hole of the shield is fixed at $r_{ho}/r_o = 0.8$; **b** Minimum normalized thickness and standard deviation of the simulation results for the corresponding thickness profiles in (**a**)

3 Experimental

Figure 1b shows the actual plating cell setup that was used for the experiments. The shield was installed to the coupon holder by the use of plastic bolts and nuts (plasticnutsandbolts.com), allowing the insulating shield to rotate at the same speed as the holder. Simulation results show that the distance between the shield and the coupon surface h and the inner radius of the shield r_{ho} were the two most important geometric parameters. The distance h was controlled by the number of nuts (each is 1.2 mm thick). Insulating shields with varying inner radii were made from plexiglass (ePlastics) the by use of a laser cutter. For each of the other geometric parameters, values that were considered in the simulations were constrained in part by factoring in considerations such as ease of fabrication and are listed in Table 1. The distance between the anode and the shield is set to $\sim$50 mm so that the impact of the anode on the current distribution on the cathode can be safely ignored.

Copper was electrodeposited at 25 °C from a plating bath containing 0.63 M cupric sulfate ($CuSO_4{\cdot}5H_2O$, Fisher Scientific) and 0.3 M sulfuric acid (H_2SO_4, EMD Chemicals). This electrolyte composition has been widely

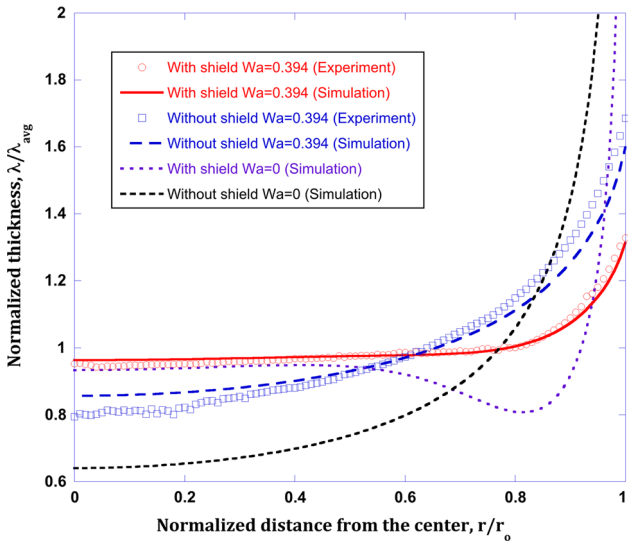

Fig. 4 Comparison of simulation and experimental results ($Wa = 0.394$) for $h/r_o = 0.24$ and $r_{ho}/r_o = 0.8$ and for a shield-free RDE. To emphasize the impact on uniformity of electrode kinetics, the simulation results when $Wa = 0$ are also shown

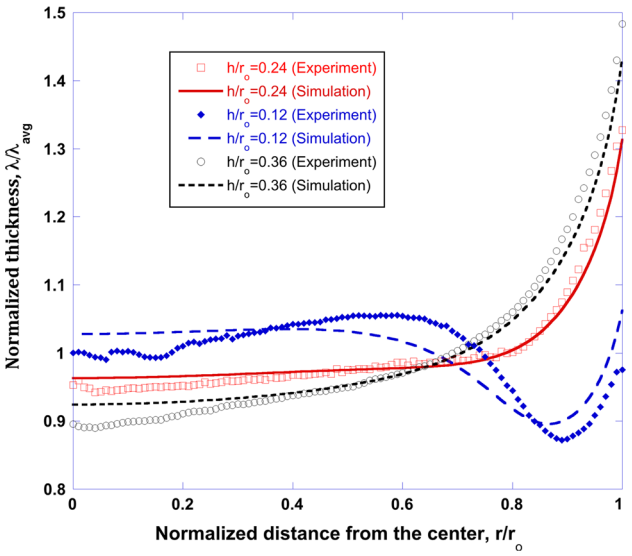

Fig. 5 Comparison of simulation and experimental results for $r_{ho}/r_o = 0.8$, $Wa = 0.394$ and three shield distances h/r_o

used in the Cu electrodeposition process and has a current efficiency of nearly 100 %. The electrical conductivity of this electrolyte at 25 °C has been reported to be 115 mS/cm [14]. By setting the cathodic charge transfer coefficient α_c to 0.5, the Wagner number of the experiment calculated from Eq. (6) is 0.394.

The electrodeposition experiments were controlled using an EcoChemie type III μ Autolab potentiostat. The Cu film was deposited galvanostatically at the cathodic current density of -15 mA/cm^2. The plating time was calculated through Faraday's law to deposit a Cu film with an average thickness of 5,000 nm assuming 100 % current efficiency. The rotation speed of the coupon holder was 300 rpm. The working electrode (WE) was a 2.5 cm × 2.5 cm coupon cleaved from a Si wafer with a Cu seed layer (45 nm thick) on the surface. The WE was attached to the coupon holder with copper tape to provide good electrical conductivity. Kapton tape was used to cover part of the wafer coupon, leaving an exposed circular region with a radius of 10 mm in the center to fix the effective WE area. The counter electrode (CE) was a platinum mesh (Fisher Scientific) located at the bottom of the plating bath container, facing directly toward the shield at a distance of ~50 mm. The plating bath container was a beaker with a volume of 1,000 mL. The WE was removed from the plating cell within 1 s of completion of the electrodeposition experiment, rinsed with deionized (DI) water, and then dried with pure nitrogen gas (N_2, Tech Air). Then half of the circular Cu deposit on the sample was covered with Kapton tape, and the other half was completely removed by immersion into 70 % nitric acid (HNO_3, Alfa Aesar) to "expose" the center point of the circular deposit for the thickness profile measurement.

The thickness profile from the center of the Cu deposit to the edge was measured by a Dektak III profilometer. For each sample, three measurements along three different radial directions were made. For each experiment, at least three samples were made to evaluate data reproducibility.

The rotating disk electrode (RDE) provides a means of easily achieving uniform and reproducible mass-transfer rates to an electrode surface. The shield, which rotates with the disk, can be anticipated to have an impact on the near-surface hydrodynamics and mass transfer. We have characterized mass transfer experimentally using a ferri-ferrocyanide redox couple to show that the effective mass-transfer-boundary-layer thickness scales with the inverse of the square root of rotation speed, as predicted by the Levich equation. This provides a measure of the spatial average. Electropolishing of copper under conditions of mass-transfer control [11], followed by profilometry, provides a means of mapping out the uniformity in mass-transfer rate.

To measure the Levich plots, a nickel RDE with the same radius $r_o = 10$ mm was made by electrodepositing a Ni film on the WE (same WE preparation process as described above) from a Watts (sulfate/chloride) nickel bath at a cathodic current density of -10 mA/cm^2 at 60 °C for ~90 min with a rotation speed of 400 rpm. This process is reported to result in ~20 μm Ni coating [10]. Then the Ni RDE was immersed in an electrolyte with 1 mM potassium ferricyanide ($K_3[Fe(CN)_6]$, Fisher Scientific), 10 mM potassium ferrocyanide ($K_4[Fe(CN)_6]$, Fisher Scientific), and 0.5 M potassium carbonate (K_2CO_3, Fisher

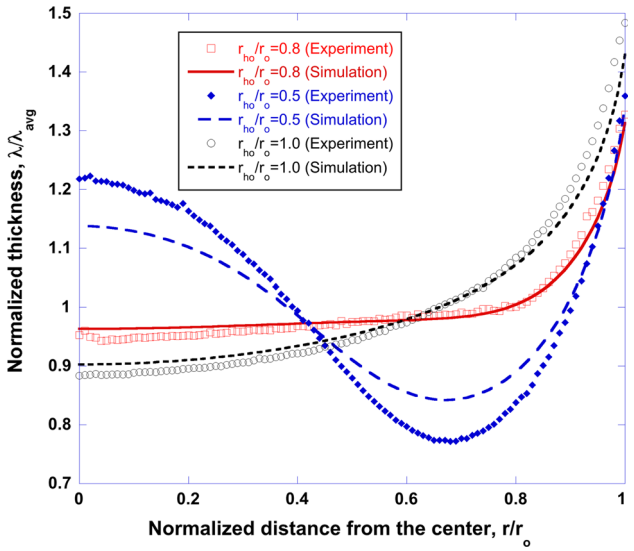

Fig. 6 Comparison of simulation and experimental results for different inner radii ($r_{ho}/r_o = 0.5$, 0.8, 1.0) with $h/r_o = 0.24$ and $Wa = 0.394$

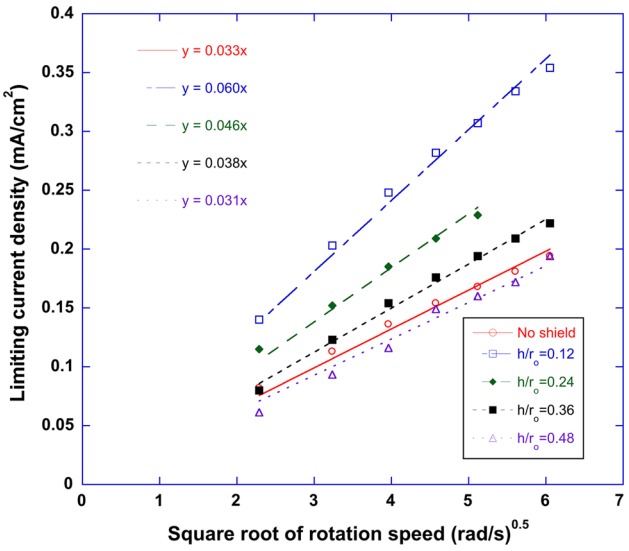

Fig. 7 Levich plots for Fe(III) reduction on the Ni RDE. Four shield-to-substrate distances were investigated: $h/r_o = 0.12$, 0.24, 0.36, and 0.48, while $r_{ho}/r_o = 0.8$

Scientific). A series of linear sweep voltammetry experiments were conducted from 0 V vs CE (a Pt wire) to −1.2 V vs CE for different rotation speeds. The same procedures were carried out for the shield-modified RDE with different shield-to-RDE distances.

For electropolishing experiments, a 5,000 nm thick Cu film was deposited onto a Pt RDE (Fisher Scientific) from a plating bath containing 0.63 M $CuSO_4$ and 0.3 M H_2SO_4 using a shield design that yields a relatively uniform current distribution. Then the RDE was moved to an electropolishing bath containing concentrated phosphoric acid (85 % H_3PO_4, Fisher Scientific), and the electropolishing potential determined from a linear sweep voltammetry experiment was applied. The electropolishing time was adjusted in order to oxidize approximately 1,000 nm of Cu deposit. Then the sample was removed from the electropolishing bath, washed with DI water, and dried with pure N_2. Current distribution was then measured as described above.

4 Results and Discussion

Figure 2a shows three experimental measurements along different radial directions from the center to the edge of a sample. The three measurements of the sample thickness indicate that the data are comparatively reproducible. Thus, the average is a reliable representation of the experimental data. The local thickness of the deposit is proportional to its local current density through Faraday's Law assuming 100 % current efficiency. Therefore, current distribution data from simulation can be compared with experimental measurements after normalizing both of the data sets over their own average values, respectively. Here, the average thickness of the experimental results is the linear average:

$$\lambda_{\text{avg}} = \frac{1}{N}\sum_{1}^{N}\lambda_i \tag{7}$$

in which λ_{avg} is the average thickness, N is the number of measured data points and is equal to 101, and λ_i is the thickness at the ith data point. The simulation results are then calculated in the same way to obtain the average value:

$$\frac{i(r)}{\int_{r=0}^{r=r_o} i(r)\mathrm{d}r/r_o} = \frac{\pi}{4\sqrt{1-\left(\frac{r}{r_o}\right)()^2}} \approx \frac{0.64}{\sqrt{1-\left(\frac{r}{r_o}\right)^2}} \tag{8}$$

In contrast, when simulating in axisymmetric coordinates, the spatial-average current density is properly calculated using $\frac{2}{r_o^2}\int_{r=0}^{r=r_o} i(r)r\mathrm{d}r$ which yields the well-known result $\frac{i(r)}{i_{\text{avg}}} = \frac{0.5}{\sqrt{1-r^2/r_o^2}}$ [15]. Equation (8) is used here to reflect how thickness measurements may be more commonly analyzed. Figure 2b shows that the experimental data and simulation results are in good consistency after normalization.

The distance between the shield and the coupon surface h and the inner radius of the shield r_{ho} were found to be the two most important geometric factors. Figure 3a shows multiple simulation results for various h/r_o. Figure 3b provides a summary of results by showing the minimum normalized thickness and the standard deviation for the

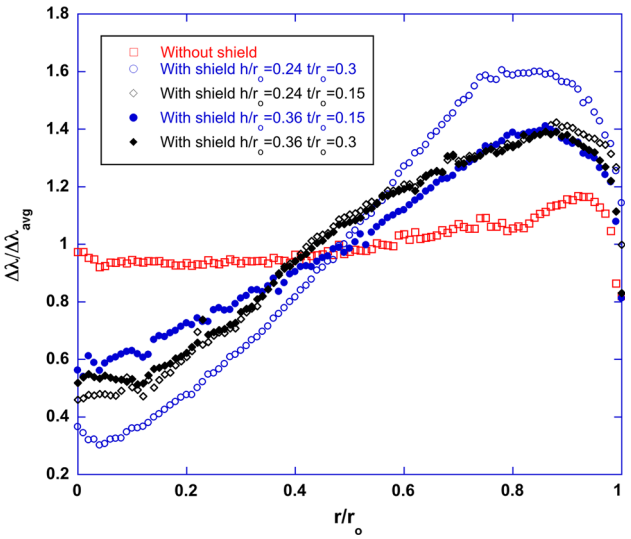

Fig. 8 Comparison between normalized mass-transfer rates obtained by electropolishing with and without a shield. In all cases, $r_{ho}/r_o = 0.8$

corresponding conditions used in Fig. 3a. Here, the standard deviation s of normalized thickness is defined as below:

$$s = \sqrt{\frac{1}{N-1}\sum_{1}^{N}\left(\frac{\lambda_i}{\lambda_{avg}} - 1\right)^2} \tag{9}$$

Depending on the application, the minimum thickness or the standard deviation may be a more relevant figure of merit. Low s and large $\lambda_{min}/\lambda_{avg}$ are indications of better current distribution uniformity. As shown in Fig. 3a, the predicted thicknesses increase significantly near the edge ($r/r_o > 0.90$) and are comparatively flat where $r/r_o < 0.75$. As the normalized distance h/r_o increases, the normalized thickness profile approaches the result without a shield. As seen in Fig. 3b, the standard deviation has a minimum value at $h/r_o = 0.15$ while the minimum normalized thickness reaches a highest value at $h/r_o = 0.35$. Combining these two results, h/r_o between 0.25 and 0.30 appears to be a good range. Experimentally, since the distance between the shield and the substrate h was controlled by the number of plastic nuts (each is 1.2 mm thick), h/r_o was set to 0.24.

As a point of comparison, the standard deviation without the shield is 0.53 and its minimum normalized thickness is 0.64. As seen in Fig. 3b, the standard deviation and minimum thickness approach the values without a shield when h/r_o increases beyond 0.8, indicating that the influence of the decreases as it is further away from the substrate. Following a similar process as described above, the optimum inner radius of the shield r_{ho}/r_o was determined to be in a range between 0.8 and 0.9.

Figure 4 shows predicted and measured normalized thickness profiles after plating with a shield with $h/r_o = 0.24$ and $r_{ho}/r_o = 0.8$. Experimentally, the estimated $Wa = 0.394$ and the kinetics resistance thus leads to an improved current distribution compared to that predicted for a primary current distribution ($Wa = 0$). Compared to the results without a shield, a more uniform current distribution is achieved. Figure 5 shows the comparison between experimental and simulation results of normalized thickness profiles when plating with the shield at different distances away from the substrate. Three distance values ($h/r_o = 0.12$, 0.24, and 0.36) have been investigated. Experimental results suggest that the distance of $h/r_o = 0.24$ leads to a more uniform current distribution.

Figure 6 shows the current distribution results for electroplating with the shields having different inner radii r_{ho}. As predicted by the simulation, the experimental data show that $r_{ho}/r_o = 0.8$ results in a more uniform current distribution with a standard deviation of 0.28 and minimum normalized thickness of 0.94. For a larger inner radius of $r_{ho}/r_o = 1$, the normalized thickness profile possesses a similar shape yet with a higher degree of non-uniformity (higher standard deviation of 0.35 and lower minimum normalized thickness of 0.90). However, for a smaller inner radius of $r_{ho}/r_o = 0.5$, the thickness profile has an above-average film thickness both in the center area ($r/r_o < 0.4$) and the area near the edge ($r/r_o > 0.9$). Consequently, the current distribution is characterized by a higher standard deviation of 0.41 and a lower minimum normalized thickness of 0.77. Therefore, other conditions held constant, $r_{ho}/r_o = 0.8$ was confirmed experimentally to lead more uniform current distribution results.

Figure 7 shows the Levich plots for Fe(III) reduction in the $K_2CO_3/K_3[Fe(CN)_6]/K_2[Fe(CN)_6]$ electrolyte with and without the shield. The slopes of all Levich plots from linear regression (with lines forced through the origin) are listed in the figure. The diffusion-limited current density on the Ni RDE without the shield is described by the Levich equation:

$$|i_L| = 0.620nFD^{2/3}\omega^{1/2}\nu^{-1/6}c_\infty = k\omega^{1/2} \tag{10}$$

in which k is the slope of the plot, $n = 1$, D is the diffusion coefficient of the Fe(III) complex, ω is the rotation speed, ν is the kinematic viscosity (0.011 cm^2/s), and c_∞ is the bulk concentration of the Fe(III) complex (1 mM).

In Fig. 7, when there is no shield, the calculated diffusion coefficient of the Fe(III) ion from the slope $k = 0.033$ is 4.20×10^{-6} cm^2/s, similar to the reported value of 3.99×10^{-6} cm^2/s [10]. The shield with the closest normalized distance from the substrate ($h/r_o = 0.12$) results in a slope of 0.060. As the distance increases, the slope decreases. When the normalized distance reaches 0.48, the slope approaches the value when there is no shield. Since

the presence of the shield does not change the physical properties (D and ν) of the same electrolyte, the change in the slope is the result of modification of the diffusion boundary-layer thickness. Generally, the mass-transfer-controlled current density can be used to estimate an average diffusion boundary-layer thickness δ

$$|i_L| = nFD\frac{C_\infty}{\delta} \quad (11)$$

When $h/r_o < 0.48$, the shield has an impact on the mass-transfer rate of the ions flowing to the substrate. The results in Fig. 7 show the impact of the shield on the mass-transfer-controlled spatial-average current density, but does not provide a measure of the radial variation.

Figure 8 shows the comparison of the normalized thickness profiles of the Cu deposit that is removed by mass-transfer-controlled electropolishing. Without a shield, the removal rate is relatively uniform as predicted by Levich. Results are shown for two distances h as well as two shield-thicknesses t. While t has negligible influence on the secondary current distribution, it has an impact under mass-transfer-controlled conditions with an increased thickness resulting in an increased deviation in mass-transfer uniformity. As shown in Fig. 8, in the absence of the shield, the thickness of the electropolished Cu is comparatively uniform ($s = 0.27$). However, when a shield is installed, the electropolishing rate in the center area ($r/r_o < 0.4$) is lower than the outer area. As distance increases, the profile becomes comparatively more uniform. When $h/r_o = 0.36$ and $t/r_o = 0.15$, the electropolished-Cu-thickness profile is the most uniform among the tested conditions. Also to be noticed is that for all of the shielded cases, a maximum mass-transfer rate is reached at $r/r_o = 0.8$ which corresponds to the edge of the inner hole of the shield.

The results in Figs. 7 and 8 show that the shield influences the mass-transfer behavior of the electrolyte near the substrate surface. This is important because the impact of additives such as levelers may be a strong function of mass-transfer rate [3]. Furthermore, the initial interactions between suppressors and accelerators in Cu deposition may depend on mass transfer [16]. Thus, the impact of the shield on the additive mass transfer may be a consideration even when operating at a small fraction of the limiting current density.

5 Conclusions

The effect of an insulating shield on the current distribution on a modified RDE was investigated by both simulation and experiments. Results are consistent and show that the insulating shield can improve current distribution uniformity. A practical way to install the shield into the plating cell is discussed. Two geometric parameters of the shield (inner hole radius r_{ho} and distance between the shield and the substrate surface h) have significant impact. When the insulating shield is close to the surface of the substrate ($h/r_o < 0.48$), the mass-transfer rate to the surface is altered and is nonuniform. This may be significant if operating at large fractions of the limiting current density or if the influence of plating additives on deposition rate is a strong function of mass transfer.

Acknowledgments The authors are very grateful to Atotech Inc. for their financial support. We also thank Qian Zhang for her experimental contributions to this study.

References

1. Keyes RW (2006) The impact of Moore's law. IEEE Solid-State Circuits Soc Newsl 11(5):25–27
2. Armini S (2011) Cu electrodeposition on resistive substrates in alkaline chemistry: effect of current density and wafer RPM. J Electrochem Soc 158(6):D390–D394
3. Bonou L et al (2002) Influence of additives on Cu electrodeposition mechanisms in acid solution: direct current study supported by non-electrochemical measurements. Electrochim Acta 47(26):4139–4148
4. Kelly JJ, Tian C, West AC (1999) Leveling and microstructural effects of additives for copper electrodeposition. J Electrochem Soc 146(7):2540–2545
5. Vas'ko VA et al (2004) Effect of organic additives on structure, resistivity, and room-temperature recrystallization of electrodeposited copper. Microelectron Eng 75(1):71–77
6. Lee J-M et al (2004) Improvement of current distribution uniformity on substrates for microelectromechanical systems. J Micro/Nanolithogr MEMS MOEMS 3(1):146–151
7. Tan Y-J, Lim KY (2003) Understanding and improving the uniformity of electrodeposition. Surf Coat Technol 167(2–3): 255–262
8. Willey MJ, West AC (2006) Microfluidic studies of adsorption and desorption of polyethylene glycol during copper electrodeposition. J Electrochem Soc 153(10):C728–C734
9. Newman J (1966) Resistance for flow of current to a disk. J Electrochem Soc 113(5):501–502
10. Szánto DA et al (2008) The limiting current for reduction of ferricyanide ion at nickel: the importance of experimental conditions. AIChE J 54(3):802–810
11. Vidal R, West AC (1995) Copper electropolishing in concentrated phosphoric acid: I. Experimental findings. J Electrochem Soc 142(8):2682–2689
12. Tobias CW, Wijsman R (1953) Theory of the effect of electrode resistance on current density distribution in electrolytic cells. J Electrochem Soc 100(10):459–467
13. Newman J, Thomas-Alyea KE (2012) Electrochemical systems. Wiley, Hoboken
14. Price D, Davenport W (1980) Densities, electrical conductivities and viscosities of $CuSO_4/H_2SO_4$ solutions in the range of modern electrorefining and electrowinning electrolytes. Metall Trans B 11(1):159–163
15. Newman J (1966) Current distribution on a rotating disk below the limiting current. J Electrochem Soc 113(12):1235–1241
16. Gallaway JW, Willey MJ, West AC (2009) Acceleration kinetics of PEG, PPG, and a triblock copolymer by SPS during copper electroplating. J Electrochem Soc 156(4):D146–D154